

1                    **Basal crevasse formation on Byrd Glacier, East**  
2                    **Antarctica, as proxy for past subglacial flooding events**

3                    **Sarah F. Child<sup>1,2</sup>, Leigh A. Stearns<sup>1,3</sup>, C. J. van der Veen<sup>4</sup>, Pedro Elósegui<sup>5,6</sup>**

4                    <sup>1</sup>Department of Geology, University of Kansas, Lawrence, KS 66045, USA

5                    <sup>2</sup>Cooperative Institute for Research in Environmental Sciences, University of Colorado, Boulder, CO  
6                    80309, USA

7                    <sup>3</sup>Center for Remote Sensing of Ice Sheets, University of Kansas, Lawrence, KS 66045, USA

8                    <sup>4</sup>Department of Geography & Atmospheric Sciences, University of Kansas, Lawrence, KS 66045, USA

9                    <sup>5</sup>Massachusetts Institute of Technology, Haystack Observatory, Westford, MA, 01886 USA

10                    <sup>6</sup>Institute of Marine Sciences, ICM-CSIC, Barcelona, Spain

11                    **Key Points:**

- 12                    • Increased tensile stress from subglacial flooding may initiate abnormally large basal  
13                    fractures.
- 14                    • We date abnormally large basal crevasses via feature tracking of overlying surface  
15                    depressions.
- 16                    • These rapid changes in glacier dynamics appear to have no effect on Byrd Glacier's  
17                    stability.

---

Corresponding author: Sarah F. Child, [sarah.child@colorado.edu](mailto:sarah.child@colorado.edu)

## Abstract

Linear elastic fracture mechanics (LEFM) suggests that short-lived flow accelerations, such as the one observed in the 2006 Byrd Glacier, East Antarctica, subglacial flooding event, can initiate abnormally large basal crevasses at the grounding line. Airborne radar measurements acquired in 2011 reveal hundreds of basal crevasses ranging in height  $\sim 40 - 335$  m. Particle tracking results show that the formation of the largest basal crevasse occurred at the grounding line during the 2006 flooding event. Very large basal crevasses form distinctive surface depressions directly overhead, which are observed along the Byrd Glacier flowline to the terminus of the Ross Ice Shelf. By using these surface depressions as proxies for abnormally large basal crevasses, we create a timeline of past subglacial flooding events on Byrd Glacier. Understanding the frequency of flooding events and their effect on glacier dynamics will help inform subglacial hydrology models and models of ice sheet stability.

## Plain Language Summary

Flooding events that occur under the Antarctic Ice Sheet are difficult to observe due to their location and a limited supply of remotely sensed data. In 2006, a flooding event occurred at Byrd Glacier that was followed by a  $\sim 10\%$  increase in the glacier's speed. At approximately the same time as the flood, an abnormally large basal crevasse formed within Byrd Glacier's grounding zone. Without monthly satellite data, we cannot be certain exactly when the speedup began and ended, but modeling results using the velocity data that we do have from December 2005 to February 2007 shows that significantly larger basal crevasses initiate during these speedups due to an increase in extensional stresses. These abnormally large basal crevasses form surface depressions directly overhead, which are observable from satellite data. We hypothesize that all surface depressions overlie abnormally large basal crevasses whose initiations are the result of speedups caused by subglacial flooding events. We use the surface depressions as proxies for past subglacial flooding events to better understand subglacial hydrology and its relationship with glacier dynamics.

## 1 Introduction

Basal crevasses are common on Antarctic ice shelves. They form when tensile stress and water pressure, which act to widen the crevasse, exceed lithostatic stress, which acts to close it (Rist et al., 1996, 2002; Van der Veen, 1998). Basal crevasses seem to form exclusively at glacier grounding lines, then advect down-flow through the ice shelf, often providing zones of weakness at which icebergs detach (Jezek, 1984; Luckman et al., 2012).

The location and geometry of basal crevasses can be mapped with ground-based or airborne radar measurements (Jezek et al., 1979; Jezek & Bentley, 1983; McGrath et al., 2012; Luckman et al., 2012; Vaughan et al., 2012). Along the Byrd Glacier flowline, radar data show that basal crevasses are neither uniformly sized nor spaced. Crevassing that does not occur at regular time intervals is the result of short-term variations in the stresses modulating crevasse initiation. Of the modulating stresses, tensile stress is the only variable that undergoes short-term variations, as exhibited by changes in ice velocity.

In this study, we investigate the formation and evolution of basal crevasses extending from the Byrd Glacier grounding line onto the Ross Ice Shelf (RIS) (Figure 1A). We identify over 300 basal crevasses within  $\sim 5$  km of the grounding line. Of the crevasses whose heights we are able to measure, 86% are shorter than 100 m, but a few crevasses, including the one closest to the grounding line, exceed 300 m in height. We hypothesize that the rapid drainage of two subglacial lakes in the Byrd Glacier catchment (Stearns

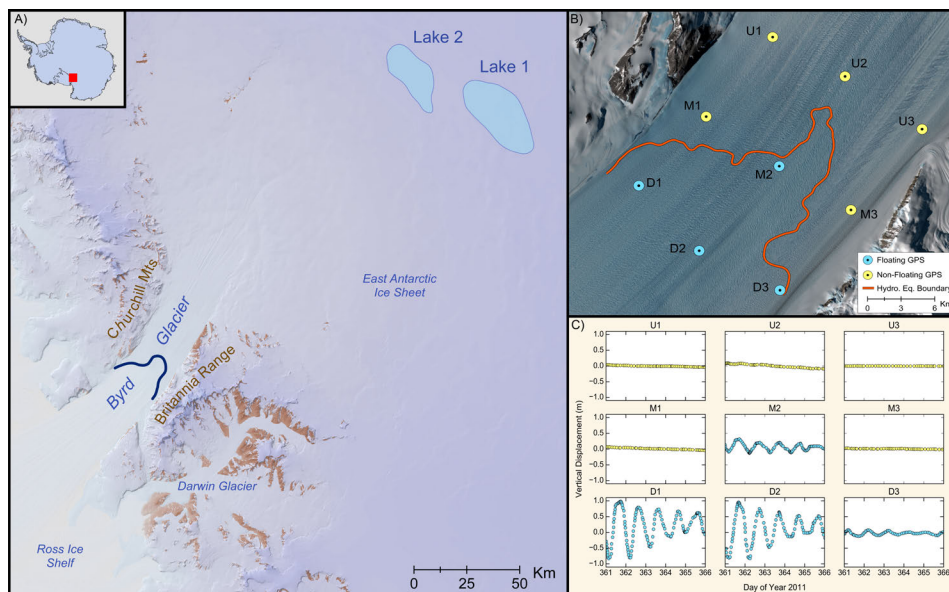


**Figure 1.** A) Map of Byrd Glacier and the subglacial lakes located  $\sim 175$  km up-flow from the grounding line (Stearns et al., 2008). The trunk of Byrd Glacier is  $\sim 25$  km wide and  $\sim 100$  km long; ice flow is from the top right to the bottom left. The background image is a hillshade made from the Polar Geospatial Center’s Regional Elevation Model of Antarctica 8 m mosaics. The grounding line, derived in section 3.1, is shown as the navy blue line. The extent of (A) is outlined in red on the inset map at the upper left-hand corner. B) The grounding zone is between the limit of tidal flexure (just down-flow of yellow GPS points) and hydrostatic equilibrium (orange line). GPS labels represent up-flow (*U*), middle (*M*), and down-flow (*D*). C) Time-varying estimates of the vertical component of site position of the nine GPS receiving systems that straddle the grounding line, for six days in December 2011.

67 et al., 2008; Carter et al., 2017) led to the formation of this anomalously large basal crevasse  
 68 at the grounding line. And, because large basal crevasses cause surface depressions, we  
 69 explore whether the train of surface depressions between Byrd Glacier and the calving  
 70 front of the Ross Ice Shelf can be used as proxies for past subglacial flooding events.

## 71 2 Data and Methods

### 72 2.1 Grounding line location

73 Basal crevasses appear to only form at the grounding line, where tensile stresses  
 74 and water pressure can exceed the lithostatic stress (Jezek & Bentley, 1983; Bentley, 1987).  
 75 The grounding line is located within a grounding zone (Figure 1), estimated through tidal  
 76 flexure (up-flow limit, where a glacier undergoes vertical displacement due to ocean tides)  
 77 and the hydrostatic equilibrium boundary (down-flow limit, where a glacier is fully float-  
 78 ing) (Vaughan, 1994; Fricker & Padman, 2006; Brunt et al., 2010). We use both *in situ*  
 79 GPS observations and airborne and satellite data to identify these limits (see supplement-  
 80 al for more information).

81

## 2.2 Basal crevasse geometry

82

### 2.2.1 Observed crevasse locations and heights

83

84

85

86

87

88

89

From December 2011 to January 2012, the Center for Remote Sensing of Ice Sheets (CReSIS) collected a dense grid of airborne radar data over Byrd Glacier. In this study, we only use the data recorded by the radar depth sounder (MCoRDS V2) operating at 180-210 MHz (Gogineni et al., 2014). The main sources of error for MCoRDS V2 are multiple reflectors, electronic noise, and off-nadir reflections (CReSIS, 2014), which is an estimated error of  $\sim 30.6$  m in thickness measurements (Gogineni et al., 2014). The elevations are referenced to the WGS84 ellipsoid.

90

91

92

93

94

95

96

We ascertain locations and heights of the basal crevasses directly from the MCoRDS V2 echograms. Basal crevasses open in the same direction as the radar flight appear as hyperbola in radar echograms and the apex of those hyperbola represents the peak of the fracture. Crevasse heights are estimated by identifying the apex and both asymptotes of a hyperbola. In some cases, basal crevasses are so numerous that the asymptotes of neighboring hyperbola intersect and estimating crevasse height is not possible. We only report crevasse heights where both asymptotes are clearly identifiable.

97

### 2.2.2 Modeled crevasse locations and heights

98

99

100

101

102

103

104

CReSIS radar data were not collected coincident with the subglacial flooding event in 2006. To determine whether conditions during flooding events could produce abnormally large basal crevasses, we model crevasse heights using linear elastic fracture mechanics (LEFM) with flood and non-flood parameters (see supplemental for more information). LEFM calculates a stress intensity factor ( $K_I$ ); when this stress intensity factor exceeds the fracture criterion, or ice toughness, then a crack will propagate (Rist et al., 1996; Van der Veen, 1998), following:

$$K_I = \int_0^{h_0} \frac{2\theta_n(z)}{\sqrt{\pi h}} G(\gamma, \lambda) dz. \quad (1)$$

105

106

107

108

109

110

111

112

113

Here,  $h_0$  is the size of the starter crack, which we set to 2 m after Rist et al. (2002) and a value of  $.155 \text{ MPa m}^{\frac{1}{2}}$  for  $K_I$  (Rist et al., 1999).  $G(\gamma, \lambda)$  is a function of  $\lambda = \frac{h}{H}$  and  $\gamma = \frac{z}{h}$ , established from fitting a polynomial curve to the modelled stress intensity values, with  $H$  the ice thickness and  $z$  the depth within the glacier (Van der Veen, 1998).  $\theta_n(z)$  represents the combined stresses (tensile, lithostatic, and water pressure) acting at the crevasse tip. Tensile stress is calculated from strain rates, following Glen's Flow Law, and using a rate factor appropriate for surface ice at  $-20^\circ\text{C}$  (after Van der Veen et al. (2014)). Strain rates were determined from velocity data collected in February 1989 to January 1990 and December 2005 to February 2007 (Stearns et al., 2008).

114

### 2.2.3 Surface depressions

115

116

117

118

119

120

121

122

Ice overlaying a large basal crevasse adjusts to hydrostatic equilibrium by forming a surface depression (Shabtaie & Bentley, 1982; Luckman et al., 2012). Several radar studies describe the relationship between surface depressions and basal crevasses (Jezek et al., 1979; Luckman et al., 2012; McGrath et al., 2012; Humbert et al., 2015). On Byrd Glacier, anomalously large basal crevasses have overlying surface depressions which are detectable from radar echograms and optical satellite imagery (see Figure 2). We use the panchromatic band from Landsat 8 OLI imagery collected in January 2016 – December 2017 to identify surface depressions.

123

124

We determine the age of the surface depressions by using a particle tracking algorithm (after Konikow and Bredehoeft (1978)) from the depressions' centroid locations

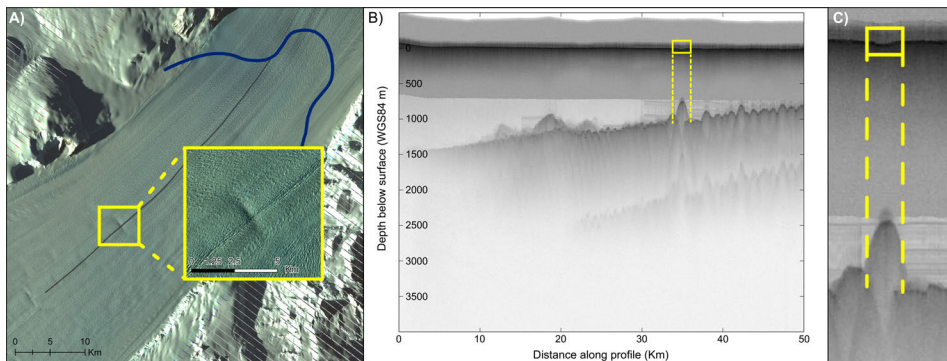


**Figure 2.** A). The surface depression overlaying a large  $\sim 290$  m tall basal crevasse (shown in panels (B) and (C)) with the CReSIS flight line in gray. The background is a Landsat 7 ETM+ image (Bands 2,3,4) acquired on February 22, 2011, approximately 10 months before CReSIS data were collected. B). Along-flow, vertical cross-section CReSIS echogram (ID: 20111205.08.003) highlighting the  $\sim 290$  m tall crevasse in yellow. C). Zoomed-in view of the  $\sim 290$  m crevasse and the overlying surface depression.

125 to the grounding line. This approach allows us to determine the flow path of each depression  
 126 and an estimate of when the crevasse formed at the grounding line. Byrd Glacier  
 127 has a lack of merging flow bands from the grounding line to the ice shelf terminus, which  
 128 suggests the glacier has maintained a consistent flow regime for the last few centuries  
 129 (Hulbe & Fahnestock, 2007; LeDoux et al., 2017). The little to no deviation in Byrd Glacier's  
 130 temporal speeds and stress regime means that accurate estimates of basal crevasse flow  
 131 advection can be determined from present-day velocity and ice flow data. The velocity  
 132 data used for particle tracking is from the Landsat Ice Speed of Antarctica (LISA; (Scambos  
 133 et al., 2019)). The LISA displacement values were generated from July 2016 to April 2017  
 134 Landsat 8 OLI imagery and has a spatial resolution of 750 m.

### 135 3 Results

#### 136 3.1 Basal crevasse geometry

137 The floating base of Byrd Glacier is heavily crevassed within the fjord and out on  
 138 RIS. Both observational and modeling results reveal that Byrd Glacier is susceptible to  
 139 crevassing of varying sizes and clusters.

##### 140 3.1.1 Observed crevasse locations and heights

141 We identify  $\sim 300$  basal crevasses from the 2011/12 CReSIS echograms (Figure 3).  
 142 Crevasse distribution is most dense within the glacier fjord, and decreases as ice flows  
 143 into the RIS. Crevasses range in height from  $\sim 40 - 335$  m and  $\sim 0.08 - 1.2$  km in width.  
 144 Hyperbole found in echograms collected near the glacier margins were ignored because  
 145 high shear stresses means those are likely Mode 2 crevasses (Van der Veen, 1998) whose  
 146 initiation is not exclusively within the grounding zone.

147 Of the  $\sim 300$  hyperbole in Figure 3, we can confidently establish the height of 107  
 148 basal crevasses where the apex and both asymptotes are clearly visible. These 100+ crevasses  
 149 are located within the region of centrally flowing ice where the primary stress is tensile  
 150 (Whillans et al., 1989) and initial crevasse propagation is due only to extensional stresses  
 151 in the direction of ice flow (Van der Veen, 1998).

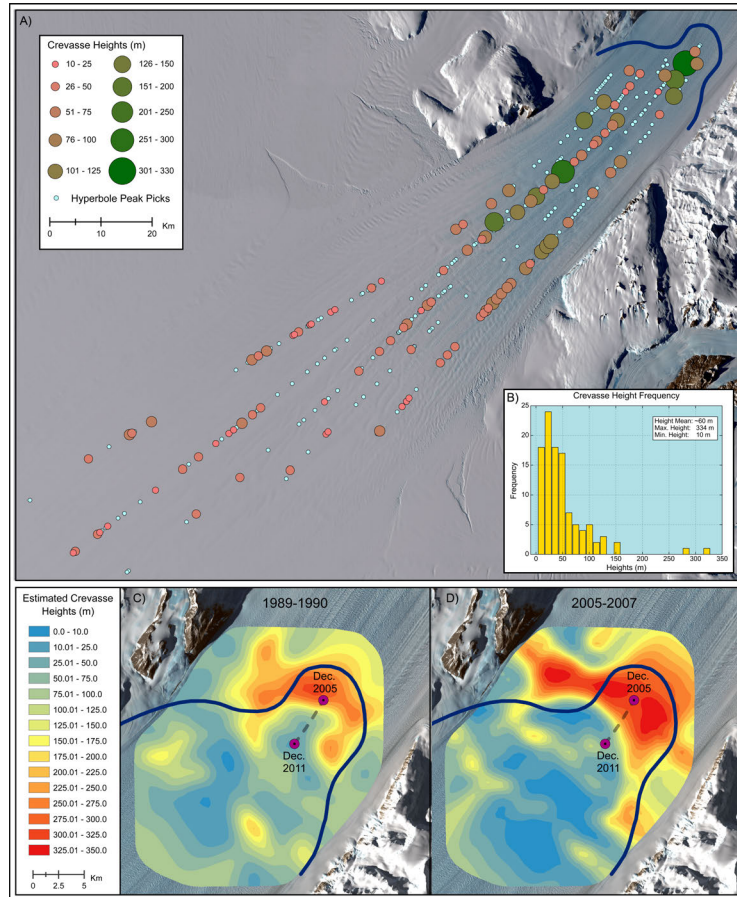


**Figure 3.** A) Heights for 107 measurable crevasses represented by the green to coral grades in color size gradients. The teal points represent all other basal crevasses. B) A frequency histogram of crevasse heights. C) and D) are the LEFM results for velocities measured in 1989 – 1990 and 2005 – 2007 respectively. The purple points in (C) and (D) represent the approximate location of the ~335 m tall basal crevasse from December 2005 to December 2011.

### 152 **3.1.2 Modeled crevasse locations and heights**

153 Due to image availability, it is impossible to pinpoint the exact timing of the ac-  
 154 celeration in 2006, but it was likely during the second half of the year (Stearns et al., 2008).  
 155 LEFM results show that during this time period, crevasse propagation heights within  
 156 the grounding zone reached  $\sim 285 - 300$  m, but only  $\sim 90 - 225$  m during a non-flooding  
 157 period. While both ice flow scenarios demonstrate the largest crevasses forming within  
 158 the up-flow limit of the grounding zone, the  $\sim 10\%$  increase in speed generates greater  
 159 tensile rates that result in a  $\sim 75$  m taller crevasse height (see Supplemental Information  
 160 for more detail).

### 161 **3.1.3 Surface depressions**

162 We identify 28 significant surface depressions over a distance of  $\sim 400$  km from Byrd  
 163 Glacier's grounding line to the RIS terminus (Figure 4). From particle tracking, the old-  
 164 est surface depression is estimated to have formed  $\sim 600$  years ago; the average interval  
 165 between surface depression formation is 22 years. Most depressions initiated at the fur-  
 166 thest up-flow point of the grounding line, but some flow-paths place initiation more south,  
 167 closer to the Churchill Mountains (Figure 1A).

168 The 2011/12 radar echograms only overlap with two surface depressions where di-  
 169 rectly beneath them are large basal crevasses,  $\sim 165$  m and  $\sim 290$  m tall. We do not ob-  
 170 serve surface depressions over shorter crevasses. Feature tracking results reveal that the  
 171  $\sim 290$  m tall crevasse formed  $\sim 1962-1963$ ; however, a surface depression was not observed  
 172 from satellite imagery until 1990. It took  $\sim 27 - 28$  years for a surface depression to form,  
 173 which aligns well with modeling efforts suggesting that viscous creep is slow at Byrd Glacier  
 174 (Van der Veen et al., 2014). The basal crevasse that formed in  $\sim 2006$  does not currently  
 175 have a corresponding depression.

## 176 **4 Discussion**

177 Basal crevasses downflow of Byrd Glacier are not of uniform height. Most crevasses  
 178 are  $< 50$  m tall (Figure 3) and do not form surface depressions. We infer the 28 observed  
 179 surface depressions overlie large basal crevasses and we hypothesize that these large basal  
 180 crevasses form during rapid subglacial drainage events (e.g. Stearns et al. (2008)). These  
 181 events cause glacier acceleration, which increases the tensile stress at the grounding line.  
 182 In addition, the large amount of water flowing across the grounding line likely enhances  
 183 melt of any pre-existing basal crevasse. Below, we outline how these two processes can  
 184 cause anomalously large basal crevasses to form during drainage events.

### 185 **4.1 Large basal crevasse formation and glacier acceleration**

186 When ice flow accelerates near the grounding line, tensile stress increases. LEFM  
 187 results illustrate that with increased tensile stress, basal crevasse heights are predicted  
 188 to be larger. Ice velocity derived from satellite remote sensing show that Byrd Glacier  
 189 can flow up to  $\sim 10\%$  faster during subglacial drainage events. This acceleration has the  
 190 potential to increase crevasse height by  $\sim 25\%$ .

191 To the best of our knowledge, the only other study to report Antarctic ice shelf basal  
 192 crevasse heights greater than 300 m is Rist et al. (2002). However, unlike the basal crevasses  
 193 initiating at Byrd Glacier, those observed by Rist et al. (2002) are rifts (Swithinbank &  
 194 Lucchitta, 1986). Rifts, though technically basal crevasses, are fractures that have prop-  
 195 agated through the entire ice thickness (Cuffey & Paterson, 2010, p.451). The observed  
 196 rifts from Rist et al. (2002) initiated from the Rutford Ice Stream and do not appear at  
 197 regular intervals along the Ronne Ice Shelf. It is probable that ice flow from Rutford Ice

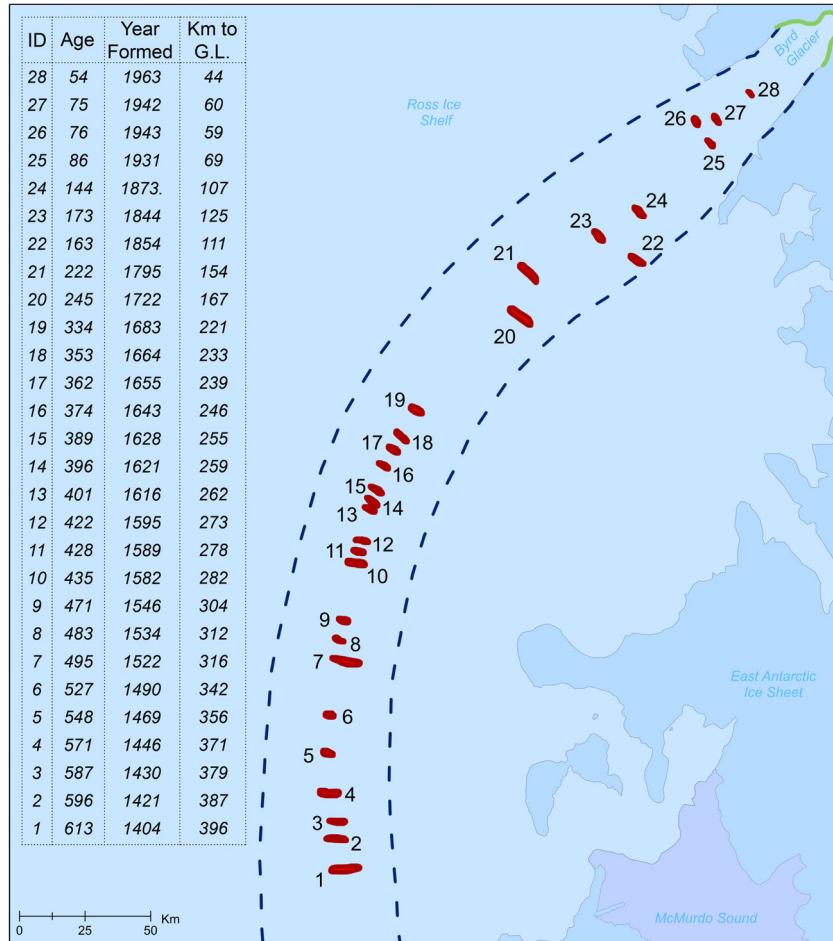


**Figure 4.** Red polygons show the locations of surface depressions extending from the Byrd Glacier grounding line to the RIS terminus. The age of individual crevasses is shown on the left side of the map; distance from the grounding line (green line) is shown on the right. The dashed blue line is the boundary of Byrd Glacier’s ice flow. We do not see any non-rift surface depressions outside of these flowlines.

Stream, like Byrd Glacier, has experienced intermittent acceleration events that have caused episodically large basal crevasses (which became full-fracture rifts).

Rist et al. (2002) hypothesized that short-term variations in ice dynamics cause abnormally large fracturing in Antarctica. While the fractures appear to persist for centuries on Byrd Glacier, they do not seem to influence its stability. On other ice shelves, such as the Larsen C Ice Shelf (Hogg & Gudmundsson, 2017) and the Filchner Ice Shelf (Ferrigno & Gould, 1987), basal crevasses become full-fracture rifts and have led to the calving of considerably large tabular icebergs. To date, no data confirms that the large basal crevasses initiated at Byrd Glacier’s grounding line have ever evolved into tabular icebergs via rifts. There is also no evidence demonstrating that Byrd Glacier’s abnormally large basal crevasses have any impact on the glacier’s or RIS’s stability.

## 4.2 Large basal crevasse formation and subglacial drainage events

LEFM underestimates the height of the  $\sim 335$  m tall crevasse by  $\sim 35 - 50$  m or  $\sim 12 - 15\%$  of the height derived from radar echograms. A possible explanation for this difference is that LEFM only predicts the initial propagation height and not the evolved height of the crevasse. The emergence of a freshwater plume at the grounding line during a subglacial flood event could have caused additional localized melting (Marsh et al., 2016).

Jenkins (2011) modelled grounding line melt rates for Byrd Glacier when a freshwater plume is the result of a subglacial lake flooding event and when the plume is due to discharge from basal deformational melt. During a flooding event, Jenkins (2011) estimates basal melt of  $15.9$  m/yr and melt of  $5.64$  m/yr from non-flood event years.

Lake 2 drained from June 2006 to March 2007 with the greatest amount of drainage occurring within the first five months (Smith et al., 2009; Stearns et al., 2008). Without knowing the month the speedup occurred, we arbitrarily designate November 2006 for the velocity increase and crevasse initiation. Assuming uniform flood influenced melt from December 2006 – March 2007 and only normal melt rates from April 2007 – November 2011, the total melt would be  $\sim 32$  m/yr. Combining that amount of deformation with the LEFM results produces a crevasse  $\sim 317 - 332$  m tall which is within  $\sim 3 - 18$  m of the tallest crevasse’s measured height.

In regards to the other abnormally large basal crevasses, it is unknown whether their initiation was also due to Lakes 1 and 2. There are several other subglacial lakes within Byrd Glacier’s basin (Smith et al., 2009) and we do not rule out the possibility they could also have caused glacier speedups. Different reservoirs and pathways of flooding basal water could be the reason surface depressions are located on discrete flow-lines.

## 4.3 Implications

Ice shelves can act as a “plug” for outlet glaciers where their presence maintains stable ice flow (Dupont & Alley, 2005; Depoorter et al., 2013). Through basal melt and iceberg calving, the majority of mass loss in Antarctica occurs at the ice shelf interface (Depoorter et al., 2013; Rignot et al., 2013). There appears to be a direct link between the stability of ice shelves and the mass balance of outlet glaciers draining into the ice shelves; following ice shelf collapses, outlet glaciers undergo sustained accelerations (Scambos et al., 2004). These events can be elicited by weakened buttressing from large calving events triggered by basal crevasses forming rifts (Rott et al., 1996; Hogg & Gudmundsson, 2017). Basal crevasses play an integral role in iceberg formation (Colgan et al., 2016) and provide greater surface area for basal melt processes (Hellmer & Jacobs, 1992).

The subglacial hydrology of Antarctica also affects ice shelf stability from grounding line drainage events. Subglacial channels on ice shelves are known to evolve and grow

246 from the influx of fresh subglacial water (Le Brocq et al., 2013; Marsh et al., 2016; Simkins  
247 et al., 2017; Dow et al., 2018) whereby increasing basal surface area for further melt to  
248 take place. These melt-induced channels are the initiating factor of forming parallel with  
249 ice-flow basal crevasses at the crest of the channels on Pine Island Glacier (Vaughan et  
250 al., 2012). This is subsequently another means of crevasse propagation as a consequence  
251 of subglacial water influx. The Antarctic basal hydraulic system influences the stabil-  
252 ity of ice shelves through its impact on glacier dynamics (speed increases leading to crevasse  
253 propagation) at the grounding line and melt rates of floating glacier ice. Having a bet-  
254 ter understanding of the drivers behind basal crevasse production has the potential to  
255 aid in better constraining of predictive models about the future of both ice shelves and  
256 ice sheets.

## 257 5 Conclusion

258 Byrd Glacier’s fjord contains an extensive number of basal crevasses—that propa-  
259 gated from tensile stresses—in a wide range of geometries. We confidently identify the  
260 heights and widths for 107 basal crevasses. The spatial pattern of the observed heights  
261 appears to be random indicating that Byrd Glacier undergoes intermittent variations in  
262 its stress regime.

263 We also detect a series of surface depressions from the fjord of Byrd Glacier to the  
264 terminus of the RIS. The depressions within the fjord are observed to directly overlay  
265 abnormally large basal crevasses; we predict that the rest of the depressions in the RIS  
266 also overlay abnormally large crevasses. Assuming basal crevasse initiation begins at the  
267 grounding line, we use feature tracking to estimate the ages of the depressions to pro-  
268 duce a timeline of abnormally large basal crevasse formation expanding over six centuries.

269 The increased tensile stresses incurred during the 2005-2007 flooding event were  
270 large enough to cause an abnormally large basal crevasse. LEFM results, in conjunction  
271 with estimated basal melt rates, agree within  $\sim 3 - 18$  m of the observed 2011 height of  
272 the  $\sim 2006$  crevasse. At present, a surface depression has not developed over this basal  
273 crevasse, but given the amount of time from crevasse inception to depression formation  
274 of the youngest surface depression (Number 28, see Figure 4), we expect a depression  
275 to form over the  $\sim 335$  m tall crevasse within the next  $\sim 12 - 13$  years.

276 We hypothesize that all abnormally large basal crevasses on Byrd Glacier form as  
277 a result of subglacial flooding speedups making basal crevasses proxies for past subglacially  
278 induced velocity increases. By tracking the present-day location of surface depressions  
279 (e.g. visible markers of abnormally large basal crevasses), to the grounding zone to mea-  
280 sure travel times, we create a timeline for 28 past subglacial flooding events.

## 281 Acknowledgments

282 This research was funded by NSF grants ANT0944087 and ANT1255488 awarded to LAS.  
283 Gordon S. Hamilton was instrumental in the collection and analysis of the GPS data.  
284 The GPS data is available from <https://www.usap-dc.org/view/project/p0000319>. The  
285 radar data was collected and generated by the Center of Remote Sensing of Ice Sheets  
286 from the support of the University of Kansas, NSF grant ANT0424589 and NASA Op-  
287 eration IceBridge grant NNX16AH54G available from: [ftp://data.cresis.ku.edu/data/rds/2011\\_Antarctica.TO](ftp://data.cresis.ku.edu/data/rds/2011_Antarctica.TO).  
288 The gridded CReSIS products are available via <ftp://data.cresis.ku.edu/data/grids/>. The  
289 surface elevation data were supplied by the Byrd Polar, Climate Research Center, and  
290 the Polar Geospatial Center under NSF-OPP awards 1543501, 1810976, 1542736, 1559691,  
291 1043681, 1541332, 0753663, 1548562, 1238993 and NASA award NNX10AN61G. The data  
292 is available through: <http://data.pgc.umn.edu/elev/dem/setsm/REMA/geocell/v1.0/2m>

293

**References**

294

Bentley, C. R. (1987). Antarctic ice streams: a review. *Journal of Geophysical Research: Solid Earth*, *92*(B9), 8843–8858.

295

296

Brunt, K. M., Fricker, H. A., Padman, L., Scambos, T. A., & O’Neel, S. (2010). Mapping the grounding zone of the Ross Ice Shelf, Antarctica, using ICESat laser altimetry. *Annals of Glaciology*, *51*(55), 71–79.

297

298

299

Carter, S. P., Fricker, H. A., & Siegfried, M. R. (2017). Antarctic subglacial lakes drain through sediment-floored canals: theory and model testing on real and idealized domains. *The Cryosphere*, *11*(1), 381–405.

300

301

302

Colgan, W., Rajaram, H., Abdalati, W., McCutchan, C., Mottram, R., Moussavi, M. S., & Grigsby, S. (2016). Glacier crevasses: Observations, models, and mass balance implications. *Reviews of Geophysics*, *54*(1), 119–161.

303

304

305

Comiso, J. C., Gersten, R. A., Stock, L. V., Turner, J., Perez, G. J., & Cho, K. (2017). Positive trend in the Antarctic sea ice cover and associated changes in surface temperature. *Journal of Climate*, *30*(6), 2251–2267.

306

307

308

CRISIS. (2014). *Antarctica 2011 Twin Otter Data, Lawrence, Kansas, USA. Digital Media*. Retrieved from <http://data.cresis.ku.edu/>

309

310

311

Cuffey, K. M., & Paterson, W. S. B. (2010). *The physics of glaciers*. Academic Press.

312

313

314

Depoorter, M. A., Bamber, J., Griggs, J., Lenaerts, J. T., Ligtnerberg, S. R., van den Broeke, M. R., & Moholdt, G. (2013). Calving fluxes and basal melt rates of Antarctic ice shelves. *Nature*, *502*, 89–92.

315

316

317

Dow, C. F., Lee, W. S., Greenbaum, J. S., Greene, C. A., Blankenship, D. D., Poinar, K., . . . Zappa, C. J. (2018). Basal channels drive active surface hydrology and transverse ice shelf fracture. *Science Advances*, *4*(6).

318

319

320

Dupont, T. K., & Alley, R. B. (2005). Assessment of the importance of ice-shelf buttressing to ice-sheet flow. *Geophysical Research Letters*, *32*(4).

321

322

323

Elósegui, P., Davis, J. L., Johansson, J. M., & Shapiro, I. I. (1996). Detection of transient motions with the Global Positioning System. *Journal of Geophysical Research: Solid Earth*, *101*(B5), 11249–11261.

324

325

326

Elósegui, P., Davis, J. L., Oberlander, D., Baena, R., & Ekström, G. (2006). Accuracy of high-rate GPS for seismology. *Geophysical Research Letters*, *33*(11).

327

328

329

Fahnestock, M., Scambos, T., Moon, T., Gardner, A., Haran, T., & Klinger, M. (2016). Rapid large-area mapping of ice flow using Landsat 8. *Remote Sensing of Environment*, *185*, 84–94.

330

331

332

Ferrigno, J. G., & Gould, W. G. (1987). Substantial changes in the coastline of Antarctica revealed by satellite imagery. *Polar Record*, *23*(146), 577–583.

333

334

335

Fretwell, P., Pritchard, H. D., Vaughan, D. G., Bamber, J. L., Barrand, N. E., Bell, R., . . . Zirizzotti, A. (2013). Bedmap2: improved ice bed, surface and thickness datasets for Antarctica. *The Cryosphere*, *7*(1), 375–393.

336

337

338

Fricker, H. A., & Padman, L. (2006). Ice shelf grounding zone structure from ICESat laser altimetry. *Geophysical Research Letters*, *33*(15).

339

340

341

Glennie, C. (2018). Arctic high-resolution elevation models: Accuracy in sloped and vegetated terrain. *Journal of Surveying Engineering*, *144*(1).

342

343

344

Gogineni, S., Yan, J.-B., Paden, J. D., Leuschen, C. J., Li, J., Rodriguez-Morales, F., . . . Gauch, J. (2014). Bed topography of Jakobshavn Isbræ, Greenland, and Byrd Glacier, Antarctica. *Journal of Glaciology*, *60*(223), 813–833.

345

346

347

Haran, T., Bohlander, J., Scambos, T., Painter, T., & Fahnestock, M. (2014). MODIS Mosaic of Antarctica 2008–2009 (MOA2009) image map, Version 1 (Updated 2019). Boulder, Colorado USA, National Snow and Ice Data Center. (Accessed: October 9, 2019) doi: <https://doi.org/10.7265/N5KP8037>

348

349

350

Hellmer, H. H., & Jacobs, S. S. (1992). Ocean interactions with the base of Amery Ice Shelf, Antarctica. *Journal of Geophysical Research: Oceans*, *97*(12).

351

352

353

Hogg, A. E., & Gudmundsson, G. H. (2017). Impacts of the Larsen-C Ice Shelf calving event. *Nature Climate Change*, *7*(8), 540–542.

- 348 Hooke, R. L. (1981). Flow law for polycrystalline ice in glaciers: comparison of the-  
 349 oretical predictions, laboratory data, and field measurements. *Reviews of Geo-*  
 350 *physics*, 19(4), 664–672.
- 351 Howat, I. M., Porter, C., Smith, B. E., Noh, M.-J., & Morin, P. (2019). The refer-  
 352 ence elevation model of antarctica. *The Cryosphere*, 13(2), 665–674.
- 353 Hulbe, C., & Fahnestock, M. (2007). Century-scale discharge stagnation and reac-  
 354 tivation of the Ross ice streams, West Antarctica. *Journal of Geophysical Re-*  
 355 *search: Earth Surface*, 112(3).
- 356 Humbert, A., Steinhage, D., Helm, V., Hoerz, S., Berendt, J., Leipprand, E., ...  
 357 Müller, R. (2015). On the link between surface and basal structures of the  
 358 Jelbart Ice Shelf, Antarctica. *Journal of Glaciology*, 61(229), 975–986.
- 359 Jenkins, A. (2011). Convection-driven melting near the grounding lines of ice shelves  
 360 and tidewater glaciers. *Journal of Physical Oceanography*, 41(12), 2279–2294.
- 361 Jenson, S. K., & Domingue, J. O. (1988). Extracting topographic structure from  
 362 digital elevation data for geographic information system analysis. *Photogram-*  
 363 *metric Engineering and Remote Sensing*, 54(11), 1593–1600.
- 364 Jezek, K. C. (1984). A modified theory of bottom crevasses used as a means for  
 365 measuring the buttressing effect of ice shelves on inland ice sheets. *Journal of*  
 366 *Geophysical Research: Solid Earth*, 89(3).
- 367 Jezek, K. C., & Bentley, C. R. (1983). Field studies of bottom crevasses in the Ross  
 368 Ice Shelf, Antarctica. *Journal of Glaciology*, 29(101), 118–126.
- 369 Jezek, K. C., Bentley, C. R., & Clough, J. W. (1979). Electromagnetic sounding  
 370 of bottom crevasses on the Ross Ice Shelf, Antarctica. *Journal of Glaciology*,  
 371 24(90), 321–330.
- 372 Jimenez, S., & Duddu, R. (2018). On the evaluation of the stress intensity factor in  
 373 calving models using linear elastic fracture mechanics. *Journal of Glaciology*,  
 374 64(247), 759–770.
- 375 Konikow, L. F., & Bredehoeft, J. D. (1978). *Computer model of two-dimensional so-*  
 376 *lute transport and dispersion in ground water* (Vol. 2) (No. 7). US Government  
 377 Printing Office Washington, DC.
- 378 Lai, C.-Y., Kingslake, J., Wearing, M. G., Chen, P.-H. C., Gentine, P., Li, H.,  
 379 ... van Wessem, J. M. (2020). Vulnerability of Antarctica’s ice shelves to  
 380 meltwater-driven fracture. *Nature*, 584(7822), 574–578.
- 381 Le Brocq, A. M., Ross, N., Griggs, J. A., Bingham, R. G., Corr, H. F., Ferraccioli,  
 382 F., & Jenkins, A. (2013). Evidence from ice shelves for channelized meltwater  
 383 flow beneath the Antarctic Ice Sheet. *Nature Geoscience*, 6(11), 945–948.
- 384 LeDoux, C. M., Hulbe, C. L., Forbes, M. P., Scambos, T. A., & Alley, K. (2017).  
 385 Structural provinces of the Ross Ice Shelf, Antarctica. *Annals of Glaciology*,  
 386 58(75pt1), 88–98.
- 387 Lichten, S. M., & Border, J. S. (1987). Strategies for high-precision Global Position-  
 388 ing System orbit determination. *Journal of Geophysical Research: Solid Earth*,  
 389 92(B12), 12751–12762.
- 390 Livingstone, S., Clark, C., Woodward, J., & Kingslake, J. (2013). Potential sub-  
 391 glacial lake locations and meltwater drainage pathways beneath the Antarctic  
 392 and Greenland ice sheets. *Cryosphere*, 7(6), 1721–1740.
- 393 Luckman, A., Jansen, D., Kulesa, B., Edward King, P., & Benn, D. (2012). Basal  
 394 crevasses in Larsen C Ice Shelf and implications for their global abundance.  
 395 *The Cryosphere*, 6(1), 113–123.
- 396 Marsh, O. J., Fricker, H. A., Siegfried, M. R., Christianson, K., Nicholls, K. W.,  
 397 Corr, H. F., & Catania, G. (2016). High basal melting forming a channel at  
 398 the grounding line of Ross Ice Shelf, Antarctica. *Geophysical Research Letters*,  
 399 43(1), 250–255.
- 400 McGrath, D., Steffen, K., Scambos, T., Rajaram, H., Casassa, G., & Lagos, J. L. R.  
 401 (2012). Basal crevasses and associated surface crevassing on the Larsen C ice  
 402 shelf, Antarctica, and their role in ice-shelf instability. *Annals of Glaciology*,

- 403 53(60), 10–18.
- 404 McNabb, R. (2019). *Pybob: A python package of geospatial tools*. Github. Retrieved  
405 from <https://github.com/iamdonovan/pybob> (Version 0.25)
- 406 Noh, M.-J., & Howat, I. M. (2015). Automated stereo-photogrammetric DEM  
407 generation at high latitudes: Surface Extraction with TIN-based Search-space  
408 Minimization (SETSM) validation and demonstration over glaciated regions.  
409 *GIScience and Remote Sensing*, 52(2), 198–217.
- 410 Nuth, C., & Kääb, A. (2011). Co-registration and bias corrections of satellite eleva-  
411 tion data sets for quantifying glacier thickness change. *The Cryosphere*, 5(1),  
412 271–290.
- 413 O’Callaghan, J. F., & Mark, D. M. (1984). The extraction of drainage networks  
414 from digital elevation data. *Computer Vision, Graphics, and Image Processing*,  
415 28(3), 323–344.
- 416 Pavlis, N. K., Holmes, S. A., Kenyon, S. C., & Factor, J. K. (2012). The develop-  
417 ment and evaluation of the Earth Gravitational Model 2008 (EGM2008). *Jour-  
418 nal of Geophysical Research: Solid Earth*, 117(B4).
- 419 Rignot, E., Jacobs, S., Mouginot, J., & Scheuchl, B. (2013). Ice-shelf melting around  
420 Antarctica. *Science*, 341(6143), 266–270.
- 421 Rist, M., Sammonds, P., Murrell, S., Meredith, P., Doake, C., Oerter, H., & Mat-  
422 suki, K. (1999). Experimental and theoretical fracture mechanics applied to  
423 Antarctic ice fracture and surface crevassing. *Journal of Geophysical Research:  
424 Solid Earth*, 104(B2), 2973–2987.
- 425 Rist, M., Sammonds, P., Murrell, S., Meredith, P., Oerter, H., & Doake, C. (1996).  
426 Experimental fracture and mechanical properties of Antarctic ice: preliminary  
427 results. *Annals of glaciology*, 23, 284–292.
- 428 Rist, M., Sammonds, P., Oerter, H., & Doake, C. (2002). Fracture of Antarctic  
429 shelf ice. *Journal of Geophysical Research: Solid Earth*, 107(1), ECV 2.1–ECV  
430 2.13.
- 431 Rott, H., Skvarca, P., & Nagler, T. (1996). Rapid collapse of northern Larsen ice  
432 shelf, Antarctica. *Science*, 271(5250), 788–792.
- 433 Sandhäger, H., Rack, W., & Jansen, D. (2005). Model investigations of larsen b ice  
434 shelf dynamics prior to the breakup. *FRISP Rep*, 16, 5–12.
- 435 Scambos, T. A., Bohlander, J., Shuman, C., & Skvarca, P. (2004). Glacier ac-  
436 celeration and thinning after ice shelf collapse in the Larsen B embayment,  
437 Antarctica. *Geophysical Research Letters*, 31(18).
- 438 Scambos, T. A., Dutkiewicz, M. J., Wilson, J. C., & Bindschadler, R. A. (1992).  
439 Application of image cross-correlation to the measurement of glacier velocity  
440 using satellite image data. *Remote sensing of environment*, 42(3), 177–186.
- 441 Scambos, T. A., Fahnestock, M., Moon, T., Gardner, A., & Klinger, M. (2019). *Ice  
442 Speed of Antarctica (LISA), Version 1. [2016-2017]*. Retrieved from [https://  
443 doi.org/10.7265/nxpc-e997](https://doi.org/10.7265/nxpc-e997).
- 444 Shabtaie, S., & Bentley, C. R. (1982). Tabular icebergs: implications from geophysi-  
445 cal studies of ice shelves. *Journal of Glaciology*, 28(100), 413–430.
- 446 Shreve, R. L. (1972). Movement of water in glaciers. *Journal of Glaciology*, 11(62),  
447 205–214.
- 448 Simkins, L. M., Anderson, J. B., Greenwood, S. L., Gonnermann, H. M., Prothro,  
449 L. O., Halberstadt, A. R. W., . . . DeConto, R. M. (2017). Anatomy of a melt-  
450 water drainage system beneath the ancestral East Antarctic ice sheet. *Nature  
451 Geoscience*, 10(9), 691–697.
- 452 Smith, B. E., Fricker, H. A., Joughin, I. R., & Tulaczyk, S. (2009). An inventory of  
453 active subglacial lakes in Antarctica detected by ICESat (2003–2008). *Journal  
454 of Glaciology*, 55(192), 573–595.
- 455 Stearns, L. A., Smith, B. E., & Hamilton, G. S. (2008). Increased flow speed on  
456 a large East Antarctic outlet glacier caused by subglacial floods. *Nature Geo-  
457 science*, 1(12), 827–831.

- 458 Swithinbank, C., & Lucchitta, B. K. (1986). Multispectral digital image mapping of  
459 Antarctic ice features. *Annals of glaciology*, *8*, 159–163.
- 460 Tinto, K. J., Padman, L., Siddoway, C. S., Springer, S. R., Fricker, H. A., Das, I., ...  
461 Bell, R. E. (2019). Ross Ice Shelf response to climate driven by the tectonic  
462 imprint on seafloor bathymetry. *Nature Geoscience*, *12*(6), 441–449.
- 463 Van der Veen, C. J. (1998). Fracture mechanics approach to penetration of bottom  
464 crevasses on glaciers. *Cold Regions Science and Technology*, *27*(3), 213–223.
- 465 Van der Veen, C. J. (2013). *Fundamentals of glacier dynamics*. CRC press.
- 466 Van der Veen, C. J., Stearns, L. A., Johnson, J. T., & Csatho, B. M. (2014). Flow  
467 dynamics of Byrd Glacier, East Antarctica. *Journal of Glaciology*, *60*(224),  
468 1053–1064.
- 469 Van der Veen, C. J., & Whillans, I. M. (1989). Force budget: I. Theory and numeri-  
470 cal methods. *Journal of Glaciology*, *35*(119), 53–60.
- 471 Vaughan, D. G. (1994). Investigating tidal flexure on an ice shelf using kinematic  
472 GPS. *Annals of Glaciology*, *20*, 372–376.
- 473 Vaughan, D. G., Corr, H. F., Bindschadler, R. A., Dutrieux, P., Gudmundsson,  
474 G. H., Jenkins, A., ... Wingham, D. J. (2012). Subglacial melt channels and  
475 fracture in the floating part of Pine Island Glacier, Antarctica. *Journal of*  
476 *Geophysical Research: Earth Surface*, *117*(F3).
- 477 Whillans, I., Chen, Y., Van der Veen, C. J., & Hughes, T. (1989). Force budget: III.  
478 Application to three-dimensional flow of Byrd Glacier, Antarctica. *Journal of*  
479 *Glaciology*, *35*(119), 68–80.